Journal of King Saud University – Science 34 (2022) 102267

HOSTED BY

Contents lists available at ScienceDirect

Journal of King Saud University – Science

journal homepage: www.sciencedirect.com

Original article

Multispectroscopic and molecular docking studies on the interaction of diltiazem hydrochloride with bovine serum albumin and its application to the quantitative determination of diltiazem hydrochloride

Nafisur Rahman [a,*], Nabila Khalil [a], Sumaiya Khan [a], Mikhlid H. Almutairi [b], Bader O. Almutairi [b], Mahboob Alam [c]

[a] Department of Chemistry, Aligarh Muslim University, Aligarh 202002, India
[b] Zoology Department, College of Science, King Saud University, P.O. Box: 2455, 11451 Riyadh, Saudi Arabia
[c] Division of Chemistry and Biotechnology, Dongguk University, 123 Dongdae-ro, Gyeongju 780714, Republic of Korea

ARTICLE INFO

Article history:
Received 9 June 2022
Revised 15 July 2022
Accepted 1 August 2022
Available online 5 August 2022

Keywords:
Diltiazem hydrochloride
Bovine serum albumin
Binding
Fluorescence
Quantification

ABSTRACT

The interaction between diltiazem hydrochloride (DTZ) and bovine serum albumin (BSA) was probed by fluorescence, UV–vis absorption, Fourier transform infrared, circular dichroism spectroscopies and molecular docking analysis at pH = 7.4. The decrease in Stern-Volmer quenching constants with rising temperature illustrated the static nature of fluorescence quenching. The distance between DTZ and BSA was evaluated and found to be 1.40 nm. The thermodynamic parameters such as ΔG, ΔH and ΔS were computed which illustrated the spontaneous and endothermic nature of binding of DTZ with BSA. Molecular docking evaluation indicated that DTZ fits into the binding pocket of subdomain I-B (site III). A spectrofluorimetric method was developed based on fluorescence quenching of BSA by DTZ to quantify diltiazem in tablets.

1. Introduction

Hypertension is considered as a major health challenge due to its propagation worldwide and causing ischaemic heart diseases and acute kidney diseases. Diltiazem hydrochloride (DTZ) is a medication used not only in the treatment of hypertension but also to cure angina pectoris (Markham and Brogden, 1993). After oral administration, three metabolites namely O-desacetyl diltiazem, *N*-desmethyl-O-desacetyl diltiazem and *N*-desmethyl diltiazem were formed which are pharmacologically active (Dasandi and Shah, 2009). The purity of active pharmaceutical ingredients ensures the quality of the drug, which enhances the remedial effect and decreases the toxicity. Therefore, an analytical investigation of drug substances and their related impurities is necessary. Several analytical methods have been developed to quantify active pharmaceutical ingredients, impurities, metabolites and degradation products in different matrices (Rahman and Azmi, 2000a; Rahman et al., 2006, 2007; AlOthman et al., 2013; Siddiqui et al., 2017; Husain et al., 2021).

Serum albumin serves as carrier protein due to its large abundance and hence transport drug molecule to its site of action (Sood et al., 2018). The literature survey revealed that the structural analogy between bovine serum albumin (BSA) and human serum albumin (HSA) makes BSA an ideal protein to assess the drug protein interaction (Guo et al., 2009). It was also stated that the similarity between BSA and HSA in terms of amino acid sequence and identity is about 86% and 75.6%, respectively (Siddiqui et al., 2021). BSA is made up of a single chain of about 583 amino acid residues. The amino acid chain is consisting of 3 homologous but structurally different domains (I, II, III) (Fig. S1). These domains are further segregated into 9 loops by disulfide bonds. The drug binding property of BSA provides pharmacokinetic and pharmacodynamic data of drug molecules (Monirinasab et al., 2022).

The binding affinity of drug molecules to serum albumin may have direct effect on absorption, distribution, metabolism and excretion (Shi et al., 2018). The reaction of astilbin with BSA was probed by different spectroscopic approaches to gather

* Corresponding author.
E-mail address: nafisurrahman05@gmail.com (N. Rahman).
Peer review under responsibility of King Saud University.

Production and hosting by Elsevier

https://doi.org/10.1016/j.jksus.2022.102267
1018-3647/

information about the binding forces and conformational changes in BSA (Liu et al., 2018). Bao et al. (2018) have investigated the interaction between DTZ and BSA by fluorescence spectroscopy only. However, they have not studied in detail on DTZ-BSA interactions involving multi-spectroscopic approaches with molecular docking. The studies based on multi-spectroscopic techniques and molecular docking are useful to understand the binding sites for DTZ in the protein and stability of docked DTZ-protein system. Circular dichroism spectra illustrated the secondary structural changes in BSA on interaction with DTZ but this technique was not used by Bao et al.

The purpose of this work was to systematically probe the interaction of DTZ with BSA employing multi-spectroscopic methods and molecular docking. The binding mechanism was examined on the basis of thermodynamic studies of BSA-DTZ complex at different temperatures. Synchronous fluorescence, FTIR and circular dichroism spectroscopy were used to examine the conformation change of BSA due to complex formation with DTZ. Molecular docking was used to check the binding mode. Site marker studies were conducted to validate the binding site. Additionally, a spectrofluorimetric method was developed based on DTZ-BSA interaction to determine the concentration of DTZ in tablets.

2. Experimental

2.1. Reagents and chemicals

Procurements of BSA (fraction V, about 96%) and DTZ (>99%) were done from HiMedia Laboratories (India) and Sigma Aldrich (U.S.A.), respectively. Warfarin (>98%; TCI, Japan), ibuprofen (>98%; Sigma Aldrich) and indomethacin (98.5–100.5%; Sigma Aldrich) were used for site marker studies. $NaH_2PO_4{\cdot}H_2O$ (99%) and $Na_2HPO_4{\cdot}2H_2O$ (99%) were obtained from Central Drug House (P) Ltd, India to prepare a buffer solution (pH 7.4). The stock solutions of BSA (10 μM) and DTZ (1 mg/mL) were made in phosphate buffer solution (0.1 M; pH 7.4) and distilled water, respectively.

2.2. Fluorescence measurement

All fluorescence analyses were performed using a Fluorescence Spectrophotometer (Model: 2700, Hitachi High-Tech Corporation, Tokyo, Japan) fitted with quartz cells of 1 cm and a xenon lamp. Fluorescence spectra of solutions containing 5 μM BSA and varied concentration of DTZ (5–35 μg/mL) were scanned in the emission wavelength range from 300 to 540 nm using 280 nm as excitation wavelength at 283, 298 and 308 K. The measured fluorescence intensities were corrected using Eq. (1):

$$F_{corr} = F_{obs} \times 10^{\left(\frac{A_{\lambda ex}+A_{\lambda em}}{2}\right)} \quad (1)$$

where, F_{corr} and F_{obs} are the corrected and measured fluorescence intensities, $A_{\lambda ex}$ and $A_{\lambda em}$ are absorbance at the excitation and emission wavelengths, respectively. Synchronous fluorescence spectra at $\Delta\lambda$ = 15 nm (tyrosine residue) and 60 nm (tryptophan residue) were obtained using a fixed BSA concentration (5 μM) and varying concentration of DTZ (5–35 μg/mL). The 3D fluorescence spectra of BSA (5 μM) and DTZ-BSA systems were scanned using the excitation wavelength from 220 to 500 nm and emission wavelength from 200 to 600 nm with a contour interval of 10 nm.

2.3. UV-absorption spectra

The absorption spectra of BSA (5 μM), DTZ (5–20 μg/mL) and DTZ-BSA were scanned from 200 to 350 nm using Perkin-Elmer Lamda-45 spectrometer. In DTZ-BSA system, varying concentration of DTZ was mixed with BSA (5 μM) and measured at 298 K.

2.4. Fluorescence resonance energy transfer (FRET)

The absorption spectrum of DTZ (5 μM) was measured in the wavelength range 300–550 nm whereas the fluorescence spectrum of BSA (5 μM; λ_{ex} = 280 nm) was also obtained in the same wavelength region. The overlapping of absorption spectrum of DTZ with fluorescence spectrum of BSA was utilized to compute the energy transfer.

2.5. Circular dichroism (CD)

CD experiments were conducted using Jasco J-815 circular dichroism spectrometer fitted with temperature-controlled Peltier device, 150 W Xenon arc lamp and 2.0 mm quartz cuvette. Instrument specifications were response time 1 s, scanning rate 100 nm min^{-1} and wavelength range 190–300 nm. The instrument was continuously purged with N_2 gas to remove the moisture content before and during the experiment.

2.6. Fourier transform infrared (FTIR) measurement

FTIR spectra of BSA and DTZ-BSA were scanned from 4000 to 400 cm^{-1} using FTIR spectrometer (PerkinElmer).

2.7. Molecular docking

BSA crystal structure was obtained from the protein data bank (PDB ID: 3 V03). Diltiazem structure was drawn in chemdraw 12.0 with energy minimization of MM-2 method implemented in Chem.3D Pro 12.0 and structure was saved in pdb format. Auto Dock Vina program was used for docking. All water molecules were pulled out and all polar hydrogens were added for smooth docking without hindrance. Grid parameters were set as 76 × 76 × 76 Å with grid center x = 38.078, y = 22.708, z = 40.771 to envelope all active site residues. Kollman and Gasteiger charges were added to drug and protein with Auto Dock Tools (ADT), respectively and the file was saved in pdbqt format. BSA was held as rigid whereas DTZ was flexible. Accelrys Discovery Studio 4.5 software was used to examine the energy minimized output files of the auto dock vina.

2.8. Analytical application

2.8.1. Procedure for determination of DTZ

Different concentrations of DTZ (3–50 μg/mL) were taken into various volumetric flasks (10 mL) containing a fixed BSA concentration (5 μM). The total volume was maintained at 10 mL with the phosphate buffer solution (pH 7.4). The fluorescence quenching of BSA was measured at 340 nm after excitation at 280 nm. The calibration curve was established by plotting (F_0/F) versus DTZ concentration (μg/mL). The quantity of DTZ in the sample was computed from the calibration curve.

2.8.2. Procedure of reference method (Rahman and Azmi, 2000b)

Different volumes of DTZ (1.2 mg/mL) equivalent up to 50 μg/mL were transferred into various boiling tubes followed by sodium metavanadate (2.6 mL, 0.10 M) and H_2SO_4 (4 mL, 13.0 M). The mixture was heated on water bath for 20 min and then cooled. Thereafter, solution was taken into volumetric flask (10 mL) and water was added to complete the volume. Absorbance measurement was made at 750 nm.

2.8.3. Determination of DTZ in tablets

Two commercially available tablets were separately weighed, powdered and dispersed in distilled water with shaking. The insoluble materials were isolated by filtration. The filtrate was taken

into a volumetric flask (100 mL) and diluted with distilled water. Further dilutions were made, if necessary. The determination of DTZ was carried out according to the procedure given in Section 2.8.1.

3. Results and discussion

3.1. Fluorescence quenching mechanism

BSA exhibits a fluorescence emission peak at 340 nm when excited at 280 nm while DTZ showed no intrinsic fluorescence. The fluorescence intensity of BSA decreases successively and the maximum emission wavelength moved from 340 nm to 351 nm with increasing concentration of DTZ at 298 K (Fig. 1(a)). The decrease in BSA fluorescence indicated the complex formation between DTZ and BSA. Additionally, the blue shift in maximum wavelength emission described the alteration in conformation of BSA. The blue shift also pointed towards decrease in polarity around the tryptophan residues and increase in hydrophobicity. The experiments were also conducted under the same conditions at 283 K and 308 K and it was found that the quenching decreases with increasing temperature. The fluorescence quenching caused by DTZ was analyzed by Stern-Volmer equation which is expressed as:

$$\frac{F_0}{F} = 1 + K_{SV}C_Q = 1 + k_q\tau_0 C_Q \quad (2)$$

where the fluorescence intensities of BSA with and without quencher molecule are depicted by F and F_0, respectively. K_{sv} and k_q define the Stern-Volmer quenching constant and quenching rate constant, respectively. C_Q is quencher concentration, and τ_0 is average lifetime of fluorophore molecule without a quencher and corresponds to 10^{-8} s^{-1}. The Stern-Volmer plots ($\frac{F_0}{F}$ versus C_Q) at 283, 298 and 308 K are depicted in Fig. 1(b). K_{sv} values were obtained from the linear plots and then k_q values were estimated (Table 1). The K_{sv} value shows a decreasing trend with rising temperature, suggesting the quenching process is static in nature (Liu et al., 2018). Further, the k_q values were found to be larger than the maximum scatter collision quenching constant (2.00×10^{10} mol^{-1} s^{-1}) which revealed that the fluorescence quenching was caused by complex formation. It is concluded that the static type of quenching was involved during the binding of DTZ with BSA.

The Lineweaver equation (Abdelhameed et al., 2015) was also applied to analyze the type of quenching which is expressed as:

$$(F_0 - F)^{-1} = F_0^{-1} + K_{LB}^{-1}F_0^{-1}C_Q^{-1} \quad (3)$$

The plot of $(F_0 - F)^{-1}$ vs C_Q^{-1} yields a straight line (Fig. 1(c)) which indicates static quenching. Moreover, the K_{LB} values (Table 1) decreased as the temperature rises, pointing towards static quenching.

3.2. Binding constant and binding site

The binding constant and number of binding sites for a system obeying static quenching can be obtained from Eq.4:

$$Log\left(\frac{F_0 - F}{F}\right) = \log k_a + n log[Q] \quad (4)$$

Here, k_a and n describe the binding constant and the number of binding sites, respectively. The k_a and n values were computed from log $(F_0 - F)$/F vs $log[Q]$ plots at 283, 298 and 308 K (Fig. 1d). The results are listed in Table 1. The k_a value increased as a function of temperature which suggested more stability of DTZ-BSA system at higher temperature. The k_a values were higher at all the temperatures studied which illustrated a strong interaction between BSA and DTZ. This demonstrated that DTZ could be transported by BSA via blood circulation to other organs *in vivo*. Also, the n value is almost 1 which suggested the presence of one binding site for DTZ in BSA molecule.

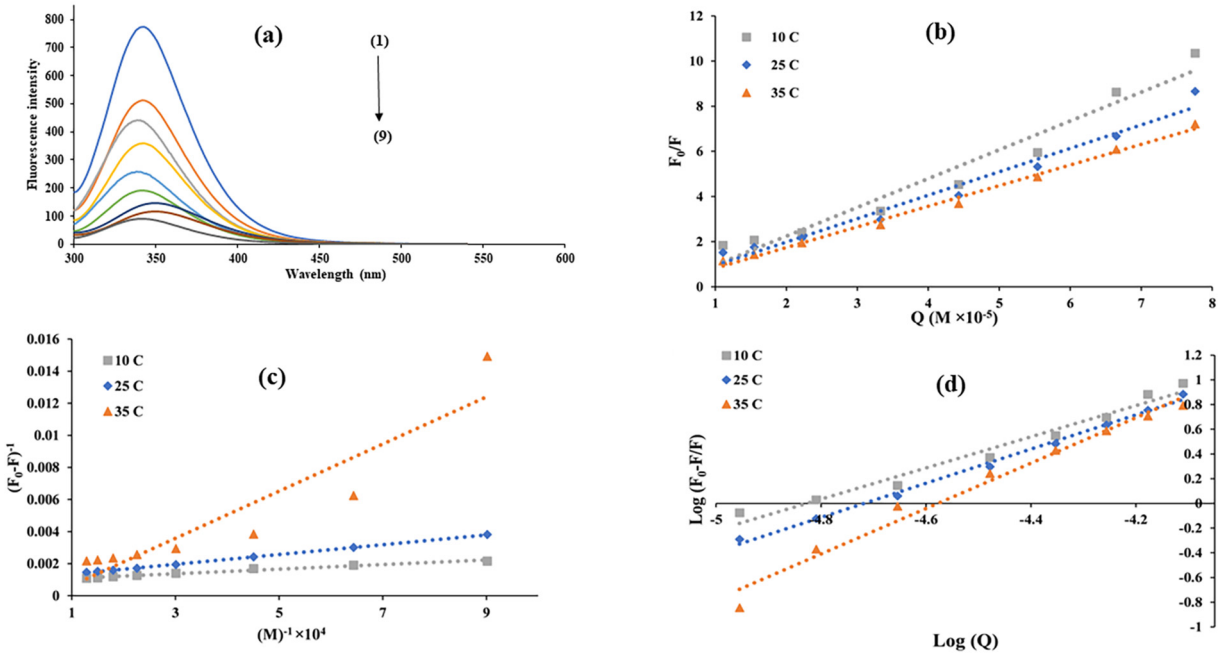

Fig. 1. (a) Fluorescence quenching spectra of BSA (b) Stern-Volmer plots for BSA-DTZ system (c) Lineweaver-Burk plots for BSA-DTZ system and (d) binding plots for BSA-DTZ system; with varying concentration of DTZ [(1) without DTZ (2) 5 μM (3) 7 μM (4) 10 μM (5) 15 μM (6) 20 μM (7) 25 μM (8) 30 μM and (9) 35 μM at pH = 7.4.

Table 1
Stern-Volmer, Lineweaver-Burk and binding constants for BSA-DTZ interacting system.

	Stern-Volmer parameters			Lineweaver-Burk parameters		Binding parameters		
Temperature (K)	K_{SV} (L/mol)	Kq (L/mol s^{-1})	R^2	K_{LB} (L/mol)	R^2	K_a (L/mol)	n	R^2
283	1.27×10^5	1.27×10^{13}	0.955	9.00×10^4	0.980	1.25×10^6	1.26	0.973
298	1.03×10^5	1.03×10^{13}	0.973	3.33×10^4	0.999	3.36×10^6	1.38	0.995
308	9.13×10^4	9.13×10^{12}	0.993	8.00×10^3	0.862	2.65×10^8	1.80	0.979

3.3. Thermodynamic study

The thermodynamic parameters such as ΔG, ΔH and ΔS were assessed at 283, 298 and 308 K using Eqs. (5) and (6):

$$\ln k = -\frac{\Delta H}{RT} + \frac{\Delta S}{R} \quad (5)$$

$$\Delta G = \Delta H - T\Delta S \quad (6)$$

The values of binding constants at 283, 298 and 308 K were obtained from Eq. (4). R is a gas constant (8.314 J mol^{-1} K^{-1}). The ΔH and ΔS values were computed from Van't Hoff plot (Fig. S2). The values of ΔG were −31.57, −40.91 and −47.14 kJ mol^{-1} at 283, 298 and 308 K, respectively which demonstrated the spontaneous nature of interaction between DTZ and BSA. The ΔH and ΔS values were computed as 144.74 kJ mol^{-1} and 0.62 kJ mol^{-1} K^{-1}, respectively. The value of ΔS indicated that the water molecules which are present in an ordered manner around the drug and protein molecules get more randomness due to hydrophobic interactions. Therefore, positive values of ΔH and ΔS illustrated the role of hydrophobic interactions in the binding of DTZ to BSA (Ross and Subramanian, 1981).

3.4. UV–Visible spectroscopy

UV–visible absorption spectra of BSA, DTZ and BSA-DTZ complex are depicted in Fig. S3. The absorption spectrum of BSA showed two bands centered at 210 nm and 280 nm. The peak at 280 nm represents the π-π* transitions arising from phenyl rings of aromatic amino acids. The peak at 210 nm characterizes the α-helical structure of BSA (Rudra et al., 2018). The addition of DTZ to BSA caused a gradual increase in absorption intensity of peak at around 210 nm with a red shift in maximum wavelength of absorption. The results confirmed the formation of complex between DTZ and BSA which also illustrated the alteration in the conformation of BSA.

3.5. Conformational studies.

3.5.1. FTIR spectroscopy

The FTIR spectrum of diltiazem hydrochloride (Fig. 2) shows a band at 1637 cm^{-1} which refers to C=O stretching. FTIR spectrum of BSA indicates the amide I band peaking at 1667 cm^{-1} which is mainly arising from C=O stretching of amide group. The band centered at 1528 cm^{-1} characterizes the amide II band which presents C—N stretching together with N—H bending. The amide I and amide II bands are considered as most valuable vibrational modes of protein backbone and are related to secondary structure of protein. The FTIR spectrum of DTZ-BSA complex revealed that the amide I band moved from 1667 cm^{-1} to 1643 cm^{-1} and amide II band disappeared which indicated that DTZ has reacted with BSA and also pointed towards the change in conformation of BSA structure.

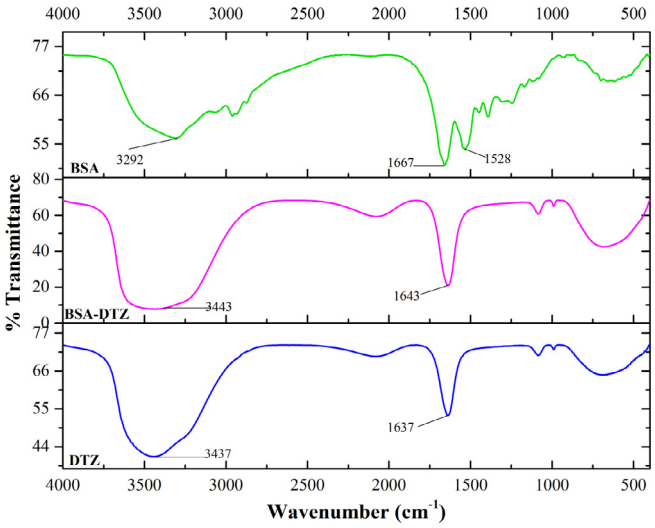

Fig. 2. FTIR Spectra of (a) BSA (b) BSA-DTZ (c) DTZ.

3.5.2. Circular dichroism spectra

CD spectra of BSA with and without DTZ at 298 K were recorded (Fig. 3). The CD spectrum of BSA exhibited two negative bands peaking at 208 nm and 222 nm which characterize the π-π* and n-π* transitions of α-helix peptide bonds, respectively. The addition of DTZ decreased the CD signal of BSA and no significant shift in band position was observed which illustrated the loss of α-helix content of BSA and alteration in protein secondary structure. These observations suggested the formation of DTZ-BSA complex. Further, α-helix content of BSA can be assessed after addition of DTZ. CD results are usually represented as mean residual ellipticity (MRE). The MRE (deg cm^2 $dmol^{-1}$) and α-helix content were quantified by Eqs. (7) and (8), respectively.

$$MRE = \frac{observedCD(mdeg)}{C_p \times n \times l \times 10} \quad (7)$$

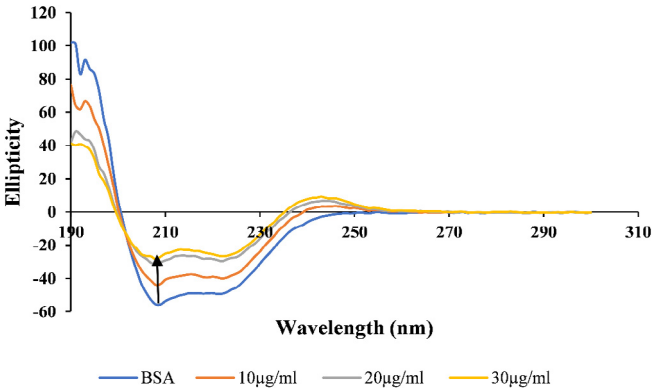

Fig. 3. CD spectra of BSA-DTZ system.

where C_p is BSA concentration (mol/L). n and l are number of amino acid residues (583), and path length (1 mm), respectively. The α-helix content of BSA and combined BSA can be computed using Eq. (8):

$$\alpha - helix = \frac{MRE_{208} - 4000}{33000 - 4000} \quad (8)$$

Herein, MRE_{208} is the experimental MRE obtained at 208 nm. The α-helix content of BSA (free) at 208 nm was 65.64%. The addition of 4.434×10^{-5} M DTZ reduces the α-helix content of BSA from 65.64% to 51.99%. Further addition of DTZ (8.87×10^{-5} M) reduced the α-helix content to 37.24%. These results suggested that the change has occurred in BSA secondary structure on interaction with DTZ.

3.5.3. Synchronous fluorescence spectra

When the Δλ value ($\lambda_{em} - \lambda_{ex}$) is held at 15 and 60 nm, the synchronous fluorescence imparts characteristic properties of tyrosine and tryptophan residues of BSA, respectively. The effect of varying concentrations of DTZ on the synchronous fluorescence of BSA is depicted in Fig. 4. It is evident that the maximum emission wavelength (λ_{em}) shifted towards longer wavelength (6.5 nm) when Δλ was set at 15 nm while a red shift of 9.5 nm in λ_{em} was noticed on setting Δλ at 60 nm upon addition of DTZ to BSA (Fig. 4b). Additionally, the synchronous fluorescence intensity of tyrosine and tryptophan residues decreased upon addition of DTZ. The results indicated the increase in polarity around tyrosine and tryptophan residues and decrease in hydrophobicity which suggested the involvement of tyrosine and tryptophan residues in binding with DTZ.

3.5.4. Three-dimensional (3D) fluorescence spectroscopy

3D fluorescence spectra and the corresponding contour plots of BSA and DTZ-BSA are displayed in Figs. 5(a) and (b) respectively, and the characteristic parameters are presented in Table 2. Peak a represents the second order scattering peak ($\lambda_{em} = 2\ \lambda_{ex}$) while peak b is related to Raleigh scattering peak ($\lambda_{em} = \lambda_{ex}$). The 3-D fluorescence spectrum also exhibited peak 1 and peak 2. Peak 1 demonstrated the fluorescence spectral nature of tryptophan and tyrosine residues. Peak 2 illustrated the fluorescence characteristics of polypeptide backbone of BSA. The fluorescence intensity of peaks 1 and 2 decreases markedly with the addition of DTZ, indicating that the protein molecule's microenvironment is changed because of complex formation.

3.6. Forster resonance energy transfer (FRET)

The overlapping of absorption spectrum of DTZ with the emission spectrum of BSA is displayed (Fig. S4). The E (Efficiency of energy transfer) value was determined using Eq. (9) (Forster, 1996).

$$E = \frac{F_O - F}{F_0} = \frac{R_0^6}{R_0^6 + r^6} \quad (9)$$

where R_0 corresponds to the critical distance at a transfer efficiency of 50% and the donor–acceptor distance is given by r. R_0 was computed using Eq. (10).

$$R_0^6 = 8.8 \times 10^{-25} k^2 N^{-4} \phi J \quad (10)$$

ϕ defines quantum yield of donor molecule, N presents medium's refractive index, k^2 is dipole's spatial orientation factor, and J is overlap integral. J can be estimated as:

$$J = \frac{\int_0^\infty F(\lambda)\varepsilon(\lambda)\lambda^4 \Delta\lambda}{\int_0^\infty F(\lambda)\Delta\lambda} \quad (11)$$

In the wavelength range λ to λ + Δλ, normalized fluorescence intensity is given by $F(\lambda)$ and the molar absorptivity of the acceptor is provided by ε(λ).

The established values of k^2, N, ϕ are 2/3, 1.36, 0.15, respectively (Senthilkumar et al., 2016). The computed values of R_0, r and J are 0.54 nm, 1.40 nm and 2.37×10^{-18} cm^3 M^{-1}, respectively. The average distance of <8 nm was obtained between the donor and acceptor, which is evidence for the transfer of energy from BSA to DTZ with high probability. The obtained r value illustrated that the reduction in the fluorescence intensity is due to static quenching mechanism (Suryawanshi et al., 2016).

3.7. Molecular docking

The 3D structure of BSA is heart-shaped with three analogous domains, which are further divided into two subdomains. Auto dock vina gives 9 different conformers of DTZ of varying Gibbs free energy that can bind with the BSA. The best fit model with minimum energy was chosen and the result shows that DTZ was mainly located at subdomain I-B (Yang et al., 2019). Fig. 6 gives 2D View of BSA-DTZ docking whereas Fig. S5 gives the detailed overview. The Gibbs free energy calculated from the docking result is slightly different from the experimental results because the X-ray crystal structure of BSA is different from that which is in the aqueous solu-

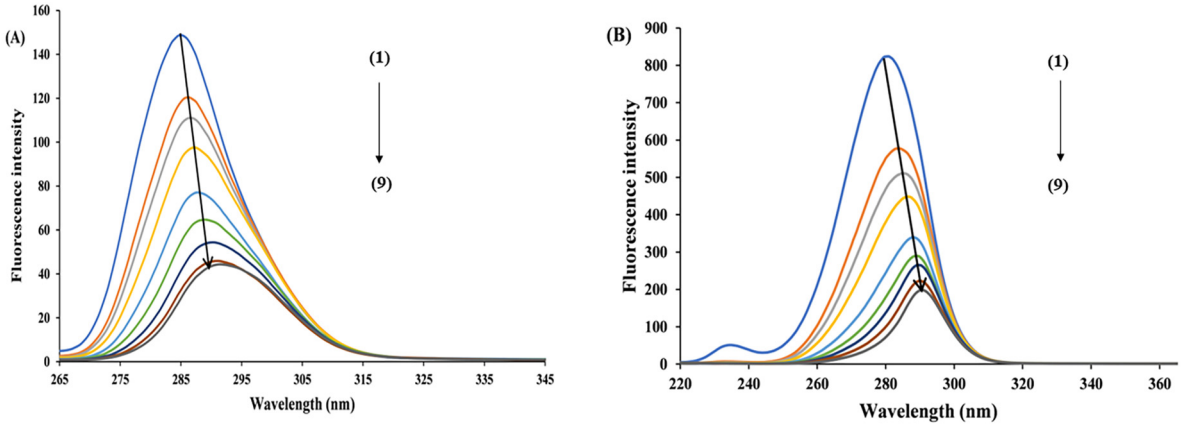

Fig. 4. Synchronous fluorescence spectra (A) at Δλ = 15 nm (B) Δλ = 60 nm for BSA-DTZ system with varying concentration of DTZ [(1) without DTZ (2) 5 μM (3) 7 μM (4) 10 μM (5) 15 μM (6) 20 μM (7) 25 μM (8) 30 μM and (9) 35 μM] at 298 K and pH = 7.4.

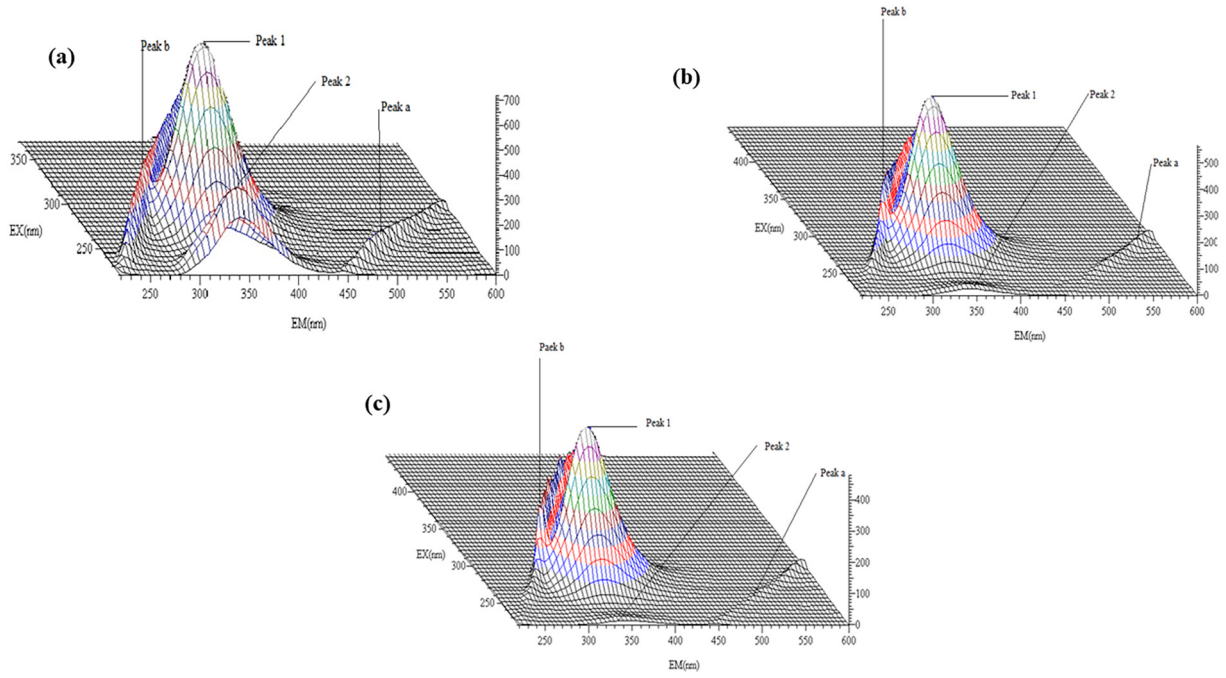

Fig. 5a. 3D fluorescence spectra of (a) BSA (5 μM), (b) BSA + 5 μg/ml DTZ, (c) BSA + 10 μg/ml DTZ.

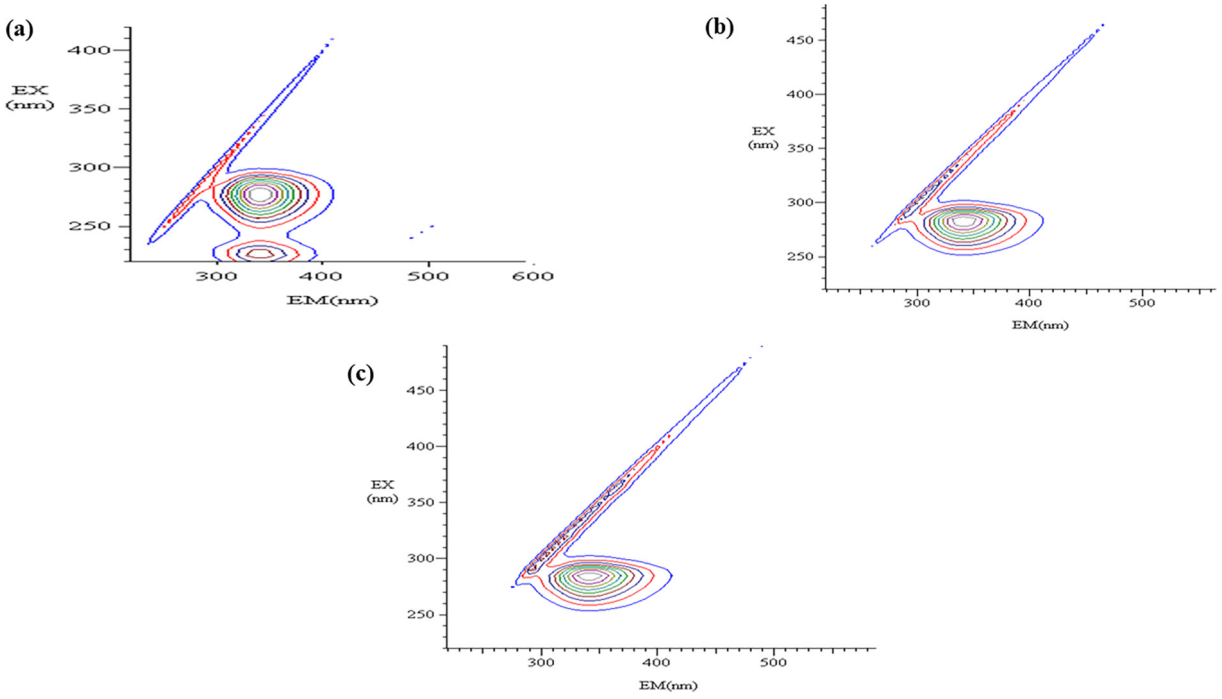

Fig. 5b. Contour plot of (a) BSA (5 μM), (b) BSA + 5 μg/ml DTZ, (c) BSA + 10 μg/ml DTZ.

tion (Neelam et al., 2010). The results of molecular docking are reported in Table S1.

3.8. Displacement studies

Competitive binding experiments were performed using indomethacin (site IB), warfarin (site IIA) and ibuprofen (site IIIA) as specific binding site markers to locate the DTZ binding site on BSA (Zsila, 2013). The protein and site probes were kept at a constant molar ratio (1:1) and DTZ was varied up to 35 μg/mL. The fluorescence spectra were obtained for BSA-DTZ system with and without site markers at 298 K.

The values of K_{sv} for BSA-DTZ in the presence of indomethacin, warfarin and ibuprofen were calculated from Stern-Volmer plots (Fig. S6) and found to be 7.30×10^3, 1.24×10^4 and 1.00×10^4-L mol^{-1}, respectively. The K_{sv} value for BSA-DTZ system without any site marker was 1.03×10^5 L mol^{-1}. On comparing the K_{sv} values, it was noticed that in presence of indomethacine K_{sv} value

Table 2
Three-dimensional fluorescence parameter.

Peaks	BSA		BSA: DTZ (1:20)			BSA: DTZ (1:40)		
	Peakposition ($\lambda_{ex}/\lambda_{em}$) nm/nm	Stokes shift	Peak position ($\lambda_{ex}/\lambda_{em}$) nm/nm	Stokes shift	Relative intensity	Peakposition ($\lambda_{ex}/\lambda_{em}$) nm/nm	Stokes shift	Relative intensity
Peak1	275/340	65	285/340	55	0.78	285/340	55	0.66
Peak2	225/340	115	225/340	115	0.08	225/345	120	0.04

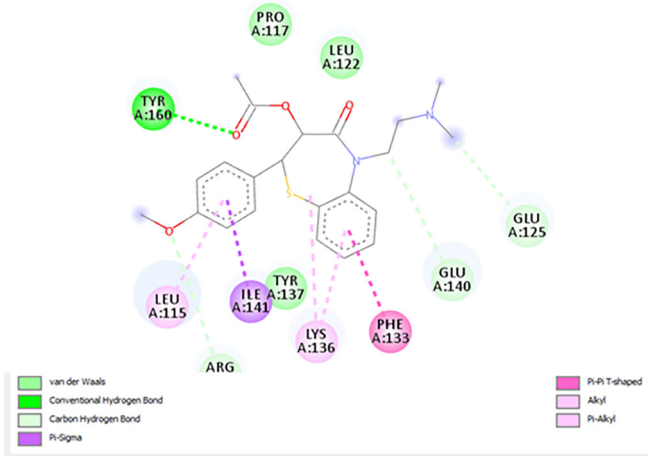

Fig. 6. 2D View of Docked structure of DTZ-BSA complex.

decreased more dramatically. These results suggested that DTZ competes with indomethacin for I-B site in BSA.

3.9. Method validation

The calibration curve (F_0/F vs concentration of DTZ) exhibited linearity in the range of 3–50 μg/mL DTZ with $R^2 > 0.99$. The detection (LOD) and quantification limits (LOQ) were evaluated using Eqs. (12) and (13) (Rahman and Khan, 2016; Lutfullah et al., 2008).

$$LOD = 3.3 \times \frac{S.D}{b} \tag{12}$$

$$LOQ = 10 \times \frac{S.D}{b} \tag{13}$$

S.D and b are standard deviation of intercept and slope of regression line, respectively. *LOD* and *LOQ* values were 0.51 μg/mL and 1.70 μg/mL, respectively.

Within-day and between-day precision were assessed with three concentrations (10,20,30 μg/ml) by performing analysis 5 times per day for within-day whereas 5 times once a day for between-day precision (Table S2). The values of RSD (%) were found in the range 0.60–0.87% and 0.71–0.89% for with-in-day and between-day precision, respectively which revealed that the proposed method has acceptable precision.

3.10. Analytical application

The proposed and reference methods were utilized to determine the quantity of DTZ in tablets. The point and interval hypothesis tests were conducted to compare the results of proposed method with the results of reference method (Table 3). At 95% confidence level, the calculated *F* and *t* (paired) values were well below the indexed values which illustrated that no significant difference occurred between the methods compared. The interval hypothesis test (Rahman and Khan, 2019) was also conducted to compare the performance of proposed and reference methods based on the true bias which was evaluated using Eq.(14):

$$\theta^2\left[\bar{X}_1^2 - \frac{S_p^2 t_{tab}^2}{n_1}\right] - 2\theta\bar{X}_1\bar{X}_2 + \left[\bar{X}_2^2 - \frac{S_p^2 t_{tab}^2}{n_2}\right] = 0 \tag{14}$$

where $\bar{X}_1$ and $\bar{X}_2$ are mean values of n_1 measurements (proposed method) and n_2 measurements (reference method), respectively. S_p and t_{tab} are pooled standard deviation and tabulated *t*-value at 95% confidence level at $n_1 + n_2 - 2$ degree of freedom. The lower limit (θ_L) and upper limit (θ_U) values (Table 3) indicated that the bias values are within ± 2%, illustrating the compliance of regulatory authorities (Acceptable methods, 1992).

4. Conclusions

The quenching of BSA fluorescence by DTZ happened through static quenching mechanism because the Stern-Volmer quenching constant decreases from 1.27×10^5 to 9.13×10^4 L mol^{-1} with increasing temperature (283–308 K). The binding constant of DTZ-BSA complex was found to be 1.25×10^6 L mol^{-1} at 298 K. The thermodynamic parameters pointed towards the spontaneous and endothermic nature of binding process. Molecular docking and displacement study indicated that DTZ fits into site IB of BSA. The calibration plot showed the linearity in the range 3–50 μg/ml DTZ with LOQ of 1.70 μg/mL. The proposed method was applied to determine diltiazem hydrochloride in tablets.

Table 3
Point and interval hypothesis test comparison of proposed and reference method at 95% confidence limit.

Formulations	Proposed method						Reference method	
	%Recovery[a]	%RSD	*t*-value[b]	F-value[b]	θ_L%	θ_U%	%Recovery	%RSD
Dilzem 30	100.0	0.02	0.16	2.19	100.00	101.52	99.6	0.08
Angizem CD 90	100.3	0.42	1.41	2.10	98.67	102.00	99.5	0.70

[a] Five independent analyses.
[b] Theoretical *t*- and *F*- values at 95% confidence level are 2.228 and 2.98, respectively.

Declaration of Competing Interest

The authors declare that they have no known competing financial interests or personal relationships that could have appeared to influence the work reported in this paper.

Acknowledgement

The authors acknowledge the Department of Chemistry, Aligarh Muslim University (A.M.U), for their kind support and instrumentation facility. Nabila Khalil acknowledges the UGC for research fellowship. The authors extend their appreciation to the Researchers Supporting Project number (RSP-2021/191), King Saud University, Riyadh, Saudi Arabia.

Appendix A. Supplementary data

Supplementary data to this article can be found online at https://doi.org/10.1016/j.jksus.2022.102267.

References

Abdelhameed, A.S., Alanazi, A.M., Kadi, A.A., 2015. Spectrofluorimetric study of finasteride and bovine serum albumin interaction and its application for quantitative determination of finasteride in tablet dosage form. Anal. Methods 12, 5096–5102.

Acceptable Methods in Drug Directorate Guidelines, 1992. Canada Health Protection Branch, Ministry of National Health and Welfare: Draft. Canada, Ottawa.

AlOthman, Z.A., Rahman, N., Siddiqui, M.R., 2013. Review on pharmaceutical impurities, stability studies and degradation products: an analytical approach. Rev. Adv. Sci. Eng. 2, 1–12. https://doi.org/10.1166/RASE.2013.1039.

Bao, C., Wang, J., Tong, X., Tang, X., Wang, Q., 2018. The Fluorescence Spectroscopic Studies on the Interaction of Diltiazem Hydrochloride with Bovine Serum Albumin. J. Appl. Life Sci. Int. 18, 1–9. https://doi.org/10.9734/jalsi/2018/43574.

Dasandi, B., Shah, S., Shivprakash. 2009. Development and validation of a high throughput and robust LC-MS/MS with electrospray ionization method for simultaneous quantitation of diltiazem and its two metabolites in human plasma: Application to a bioequivalence study. J. Chromatogr. B: Anal. Technol. Biomed. Life Sci., 877, 791–798. https://doi.org 10.1016/j.jchromb.2009.02.016.

. Modern Quantum Chemistry vol. 3, 93.

Guo, X., Zhang, L., Sun, X., Han, X., Guo, C., Kang, P., 2009. Spectroscopic studies on the interaction between sodium ozagrel and bovine serum albumin. J. Mol. Struct. 928 (2009), 114–120.

Husain, A., Iram, F., Siddiqui, A.A., Almutairi, S.M., Mohammed, O.B., Khan, S.A., Azmi, S.N.H., Rahman, N., 2021. Identification of metabolic pathways involved in the biotransformation of eslicarbazepine acetate using UPLC-MS/MS, human microsomal enzymes and in silico studies. J. King Saud Univ. Sci. 33, (2021). https://doi.org/10.1016/j.jksus.2020.101281 101281.

Liu, J., He, Y., Liu, D., He, Y., Tang, Z., Lou, H., Huo, Y., Cao, X., 2018. Characterizing the binding interaction of astilbin with bovine serum albumin: A spectroscopic study in combination with molecular docking technology. RSC Adv. 8, 7280–7286. https://doi.org/10.1039/c7ra13272g.

Lutfullah, Alam, M.N., Rahman, N., Azmi, S.N.H., 2008. Optimized and validated spectrophotometric method for the determination of uranium (VI) via complexation with meloxicam. J. Hazard. Mater. 155, 261–268. https://doi.org/10.1016/j.jhazmat.2007.11.055.

Markham, A., Brogden, R.N., 1993. Diltiazem: A review of its pharmacology and therapeutic use in older patients. Drugs Aging 3, 363–390. https://doi.org/10.2165/00002512-199303040-00007.

Monirinasab, H., Zakariazadeh, M., Kohestani, H., Kouhestani, M., Fathi, F., 2022. Study of β-lactam-based drug interaction with albumin protein using optical, sensing, and docking methods. J. Biol. Phys. 1–18. https://doi.org/10.1007/s10867-021-09599-0.

Neelam, S., Gokara, M., Sudhamalla, B., Amooru, D.G., Subramanyam, R., 2010. Interaction studies of coumaroyltyramine with human serum albumin and its biological importance, J. Phys. Chem. B. 114, 3005-3012. 10.1021/jp910156k.

Rahman, N., Azmi, S.N.H., 2000a. Extractive spectrophotometric methods for determination of diltiazem HCl in pharmaceutical formulations using bromothymol blue, bromophenol blue and bromocresol green. J. Pharm. Biomed. Anal. 24, 33–41. https://doi.org/10.1016/s0731-7085(00)00409-x.

Rahman, N., Azmi, S.N.H., 2000b. Spectrophotometric determination of diltiazem hydrochloride with sodium metavanadate. Microchem. J. 65, 39–43. https://doi.org/10.1016/S0026-265X(00)00025-4.

Rahman, N., Azmi, S.N.H., Wu, H.F., 2006. The importance of impurity analysis in pharmaceutical products: An integrated approach. Accred. Qual. Assur. 11, 69–74. https://doi.org/10.1007/s00769-006-0095-y.

Rahman, N., Azmi, S.N.H., Ahmad, Y., 2007. Quantitation of diltiazem hydrochloride in commercial dosage forms by visible spectrophotometry. J. Chinese Chem. Soc. 54, 185–196. https://doi.org/10.1002/jccs.200700059.

Rahman, N., Khan, S., 2016. Circular dichroism spectroscopy: An efficient approach for the quantitation of ampicillin in presence of cloxacillin. Spectrochim. Acta A Mol. Biomol. Spectrosc. 160, 26–33. https://doi.org/10.1016/j.saa.2016.02.009.

Rahman, N., Khan, S., 2019. Circular dichroism spectroscopy: A facile approach for quantitative analysis of captopril and study of its degradation. ACS Omega 4, 4252–4258. https://doi.org/10.1021/acsomega.8b03384.

Ross, P.D., Subramanian, S., 1981. Thermodynamics of protein association reactions: forces contributing to stability. Biochemistry 20, 3096–3102. https://doi.org/10.1021/bi00514a017.

Rudra, S., Jana, A., Sepay, N., Patel, B.K., Mahapatra, A., 2018. Characterization of the binding of strychnine with bovine β-lactoglobulin and human lysozyme using spectroscopic, kinetic and molecular docking analysis. New J. Chem. 42, 8615–8628. https://doi.org/10.1039/c8nj00810h.

Senthilkumar, R., Marimuthu, P., Paul, P., Manojkumar, Y., Arunachalam, S., Eriksson, J.E., Johnson, M.S., 2016. Plasma protein binding of anisomelic acid: spectroscopy and molecular dynamic simulations. J. Chem. Inf. Model. 5, 2401–2412. https://doi.org/10.1021/acs.jcim.6b00445.

Shi, J.H., Zhou, K.L., Lou, Y.Y., Pan, D.Q., 2018. Multi-spectroscopic and molecular modeling approaches to elucidate the binding interaction between bovine serum albumin and darunavir, a HIV protease inhibitor. Spectrochim. Acta, Part A 188, 362–371. https://doi.org/10.1016/j.saa.2017.07.040.

Siddiqui, M.R., AlOthman, Z.A., Rahman, N., 2017. Analytical techniques in pharmaceutical analysis: A review. Arabian J. Chem. 10, S1409–S1421. https://doi.org/10.1016/j.arabjc.2013.04.016.

Siddiqui, S., Ameen, F., Rehman, S., Sarwar, T., Tabish, M., 2021. Studying the interaction of drug/ligand with serum albumin. J. Mol. Liq. 336,. https://doi.org/10.1016/j.molliq.2021.116200 116200.

Sood, D., Kumar, N., Rathee, G., Singh, A., Tomar, V., Chandra, R., 2018. Mechanistic interaction study of bromo-noscapine with bovine serum albumin employing spectroscopic and chemoinformatics approaches. Sci. Rep. 8, 1–11. https://doi.org/10.1038/s41598-018-35384-6.

Suryawanshi, V.D., Walekar, L.S., Gore, A.H., Anbhule, P.V., Kolekar, G.B., 2016. Spectroscopic analysis on the binding interaction of biologically active pyrimidine derivative with bovine serum albumin. J. Pharm. Anal. 6, 56–63. https://doi.org/10.1016/j.jpha.2015.07.001.

Yang, Y., Zhang, N., Sun, Y., Li, J., Zhao, R., Zheng, Z., Ding, Y., Zhang, X., Geng, D., Sun, Y., 2019. Multispectroscopic and molecular modeling studies on the interaction of bile acids with bovine serum albumin (BSA). J. Mol. Struc. 1180, 89–99. https://doi.org/10.1016/j.molstruc.2018.09.004.

Zsila, F., 2013. Subdomain IB is the third major drug binding region of human serum albumin: toward the three-sites model. Mol. Pharmaceutics. 10, 1668–1682. https://doi.org/10.1021/mp400027q.